Journal of Optics

PAPER • OPEN ACCESS

Facet-driven formation of axial and radial In(Ga)As clusters in GaAs nanowires

To cite this article: A Balgarkashi *et al* 2020 *J. Opt.* **22** 084002

OPEN ACCESS
IOP Publishing
Journal of Optics
J. Opt. **22** (2020) 084002 (8pp)
https://doi.org/10.1088/2040-8986/ab9aad

Facet-driven formation of axial and radial In(Ga)As clusters in GaAs nanowires

A Balgarkashi[1,4], S P Ramanandan[1,4], N Tappy[1], M Nahra[3], W Kim[1], L Güniat[1], M Friedl[1], N Morgan[1], D Dede[1], J B Leran[1], C Couteau[3] and A Fontcuberta i Morral[1,2]

[1] Laboratory of Semiconductor Materials, Institute of Materials, École Polytechnique Fédérale de Lausanne (EPFL), Lausanne 1015, Switzerland
[1] Institute of Physics, École Polytechnique Fédérale de Lausanne (EPFL), Lausanne 1015, Switzerland
[3] Laboratory Light, Nanomaterials and Nanotechnologies—L2n, University of Technology of Troyes (UTT) & CNRS ERL 7004, Troyes, France

E-mail: anna.fontcuberta-morral@epfl.ch

Received 30 March 2020, revised 11 May 2020
Accepted for publication 8 June 2020
Published 1 July 2020

Abstract

Embedding quantum dots in nanowires (NWs) constitutes one promising building block for quantum photonic technologies. Earlier attempts to grow InAs quantum dots on GaAs nanowires were based on the Stranski–Krastanov growth mechanism. Here, we propose a novel strain-driven mechanism to form 3D In-rich clusters on the NW sidewalls and also on the NW top facets. The focus is on ternary InGaAs nanowire quantum dots which are particularly attractive for producing single photons at telecommunication wavelengths. In(Ga)As clusters were realized on the inclined top facets and also on the {11-2} corner facets of GaAs NW arrays by depositing InAs at a high growth temperature (630 °C). High-angle annular dark-field scanning transmission electron microscopy combined with energy-dispersive x-ray spectroscopy confirms that the observed 3D clusters are indeed In-rich. The optical functionality of the as-grown samples was verified using optical technique of cathodoluminescence. Emission maps close to the NW tip shows the presence of optically active emission centers along the NW sidewalls. Our work illustrates how facets can be used to engineer the growth of localized emitters in semiconducting NWs.

Supplementary material for this article is available online

Keywords: nanowires, heterostructure, molecular beam epitaxy, quantum dots

(Some figures may appear in colour only in the online journal)

1. Introduction

Single photon emitters (SPEs) are envisioned to play a central role in the future of quantum photonics. Their development is important for applications in quantum computation, quantum communication and quantum cryptography [1]. An ideal single-photon source is identified by a high fidelity and a high degree of anti-bunching ($g^2(0) \sim 0$), high brightness and narrow emission linewidth [2]. In recent years, bright single-photon emitters have been demonstrated by embedding semiconducting quantum dots (QDs) within nanowires (NWs) [3–6]. Semiconductor QDs are three-dimensionally confined nanostructures with discrete, atom-like emission lines. Due to quantum confinement, electronic levels in a QD can be

[4] These authors contributed equally to this work.

tuned by changing their size [7] and composition [6]. Conventional QDs are grown by planar epitaxy and embedded in a three-dimensional matrix of a higher bandgap material [8]. However, the total internal reflection at the bulk semiconductor/vacuum interface and the far-field divergence of the emission make the photon extraction highly inefficient from these structures [2, 4, 9]. NWs, on the other hand, can be designed to operate as photonic waveguides to enhance light extraction. Proper positioning of a QD on the NW axis allows the coupling of QD emission to the fundamental HE_{11} mode of the NW waveguide and coupling to other radiation modes is suppressed [4, 5, 10].

Apart from efficient light extraction, the size and morphology of the NWs offer several degrees of freedom to form low dimensional heterostructures like QDs and quantum wells (QWs). It is possible to obtain axial and radial heterostructures in NWs by varying the material composition along the axial and radial directions, respectively [11, 12]. Moreover, NWs provide a wider choice of material combinations with a higher lattice mismatch for forming axial and radial heterostructures. For instance, in the case of III–V semiconductors, one can either change the group-III element or the group-V element to form heterostructures. Some further combinations are also possible with ternary alloys consisting of an additional group-III or group-V element (e.g. InGaAs, InAsP). The large aspect ratio of NWs helps to relax the misfit strain induced by the lattice mismatch on the sidewalls and prevents the occurrence of defects [13]. Out of the available material combinations, InGaAs nanowire quantum dots (NWQDs) are particularly of interest due to their ability to emit photons in the telecommunication wavelength range and with purity in excess of 99% ($g^2(t) < 0.01$) [9, 14]. Therefore, positioning InGaAs QDs on the axis of GaAs NWs is an attractive choice to realize single-photon sources.

Most reports on the III–V QDs in NWs are based on NWs grown using gold as the catalyst. However, the incorporation of gold into the grown semiconductor is found to be detrimental for its optical properties [15]. Although self-catalysed growth of defect-free ordered GaAs NW arrays are widely reported, NW axial heterostructures based on this method is still missing. In the case of III–V semiconductors, axial heterostructures are obtained by either changing the group-III element, like GaAs/InAs, GaP/InP, or the group-V element like GaAs/GaSb. More combinations are available if either A or B is a ternary alloy. GaAs QDs in AlGaAs NWs, InAsP QDs in InP NWs, and InGaAs QDs in GaAs NWs are a few examples. Despite the availability of a wide variety of material combinations, challenges like the reservoir effect [16] and kinking [17] limit their successful implementation.

Here, we take an alternative approach for switching between two materials (InAs and GaAs). The Ga droplet, used as a growth catalyst, is completely consumed before the deposition of InAs. Formation of axial and radial localized InGaAs clusters within self-catalysed GaAs NWs is observed. Specific focus is given to the structural characterization of the obtained heterostructures using transmission electron microscopy (TEM). Our findings provide new insights into how facets can be used to engineer the growth of QDs in semiconductor NWs.

2. Experimental details

The GaAs NWs studied here were grown by the self-catalysed vapour-liquid-solid (VLS) method in a DCA P600 molecular beam epitaxy (MBE) system. A Si (111) wafer coated with an SiO_2 mask was patterned by e-beam lithography and used as the growth substrate. The NW growth was carried out at a substrate temperature of 630 °C and at Ga and As_4 beam equivalent pressures (BEPs) of 1.4×10^{-7} Torr and 2×10^{-6} Torr, respectively. The Ga supply was interrupted after an hour of NW growth. The Ga droplet used as a catalyst in the NW growth was then completely consumed under an As_4 flux of 7.2×10^{-7} Torr. InAs was deposited for 5 s at a substrate temperature of 630 °C under an As_4 BEP of 5.6×10^{-6} Torr and at a V/III ratio of 45. The morphology of the grown NW arrays was examined in a Zeiss Merlin scanning electron microscope (SEM). For structural investigation, the as-grown NWs were transferred onto a carbon-coated Cu grids and studied in a FEI Talos TEM operated at 200 keV in high-resolution and high-angle annular dark-field scanning TEM (HAADF-STEM) modes. Elemental maps were obtained by energy-dispersive x-ray (EDX) spectroscopy. The optical properties of the NWs were studied by micro-photoluminescence (μ-PL) in a cryostat operating at around 4 K under an optical excitation provided by the 632.8 nm line of He-Ne laser. The PL signal was collected into a 300 mm focal length spectrometer and dispersed by a 150 l mm^{-1} grating onto a Peltier-cooled CCD. Cathodoluminescence (CL) measurements on the NWs were carried out in an Attolight Rosa 4634 CL-SEM microscope. The measurements were carried out at 10 K with a beam energy of 5 keV and probe currents of 5–20 nA. The CL signal was collected into a 320 mm focal length spectrometer and dispersed by a 150 l mm^{-1} grating onto an IR-sensitive Peltier-cooled InGaAs PDA detector.

3. Results and discussion

Figure 1(a) shows a representative bright-field TEM micrograph of the GaAs core taken along the <1–10> zone axis. Higher magnification images of some of the specific regions along the length of the NW are shown in figures 1(b)–(d). A selected-area electron diffraction (SAED) pattern from the encircled regions in figures 1(b) and (d) is provided as an inset which reveals the crystal structure of these sections of the NW. All the NWs showed a predominantly zincblende (ZB) phase at the bottom (figure 1(b)), followed by a transition region composed of a dense region of stacking faults (figure 1 (c)). Following the transition region, the upper segment of the NWs is pure wurtzite (WZ) as shown in figure 1(d). The observed transitions in the crystal phase are due to the variation in the Ga droplet contact angle [18–20]. Variations in the droplet contact angle modify the capillary forces at the triple phase line (TPL) and control the formation of ZB and WZ phases [21].

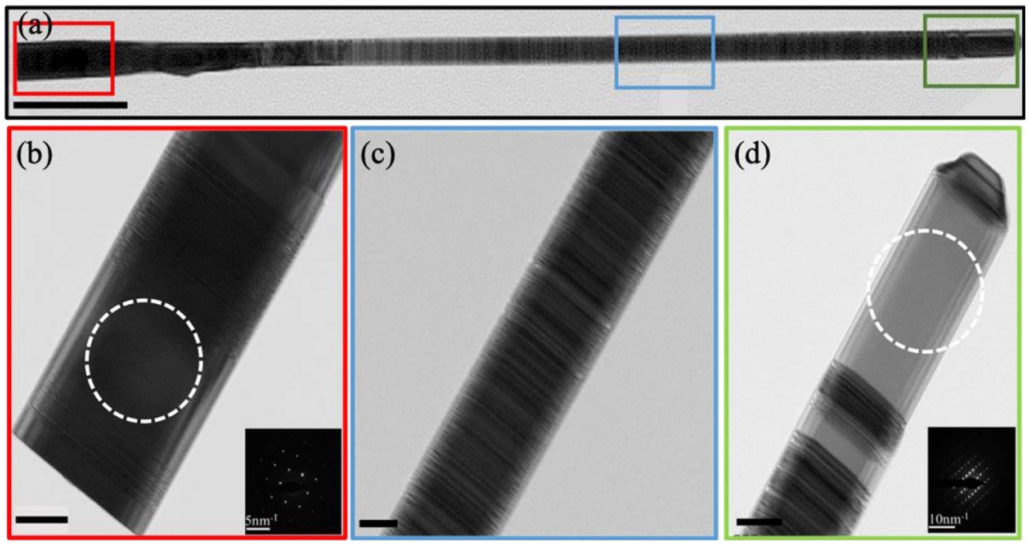

Figure 1. (a) A TEM image showing overview of a GaAs NW core viewed along the <1–10> zone axis (scale bar: 1 μm). Higher magnification images of (b) the bottom, (c) intermediate and (d) top sections of the NW as indicated in (a). The insets in (b) and (d) show the selected-area electron diffraction (SAED) pattern taken from the encircled regions (scale bars: 100 nm).

Recent *in-situ* TEM growth experiments have shown that ZB phase is favoured at small (<100°) and large (>125°) contact angles while WZ phase is favoured at any intermediate contact angle [22].

In the VLS growth of GaAs NWs, the Ga droplet acts as a non-stationary reservoir of Ga [23, 24]. The relative Ga flux during growth determines the droplet size and the contact angle. An As-rich growth condition shrinks the droplet and reduces the contact angle, whereas, a Ga-rich condition swells the droplet and increases the contact angle. Therefore, a predominantly ZB crystal structure at the bottom of the NW is due to Ga-rich conditions at the beginning of the growth. After reaching the desired length, the Ga flux is terminated, and the droplet is consumed under a constant As_4 flux. As the droplet shrinks, the contact angle also decreases gradually, creating a transition region full of stacking faults. When the contact angle falls below 125°, the WZ phase becomes favourable, and the consumption of the remaining Ga droplet results in a pure WZ phase. Finally, at a very small droplet size, the NW tip is again ZB but has a different facet morphology (figure 2). For a core–shell NW heterostructure, defects in the NW core template into the shell [25]. Thus, GaAs NW core with a defect-free tip is essential for the growth of axial heterostructures. The SEM images of the NW tip after Ga droplet consumption at 630 °C are shown in figures 2(a)–(e). Figures 2(f)–(h) show high-resolution TEM images of the NW tip taken along the <1–10> zone axis. The tilted facets are indexed by measuring the angles made with the <–1–1–1> NW growth plane. The tip of the NW showed a pure ZB phase and is free of stacking faults (figures 2(g) and (h)). However, non-uniformities in the NW tip morphology are observed. A major fraction of the NW tips observed in SEM showed a truncated pyramidal morphology with a flat triangular {111}B facet at the tip as evident in figures 2(b)–(d). The remaining fraction of NWs showed a completely pinched-off NW tip as shown in figure 2(e). In crystal growth, facet formation is governed by the slowest growing plane. Any variation in the growth conditions (like V/III ratio or temperature) affects the growth rate of different planes and dictates the final facet morphology. Under the conditions studied here, we believe the group-III and group-V re-evaporation rates to be substantial and varying from one NW to another. Therefore, the observed non-uniformities in the tip morphology can be attributed to the local variation in growth conditions.

3.1. Formation of axial In(Ga)As clusters:

Having obtained a good understanding of the GaAs NW tip morphology and crystal structure, the effect of InAs deposition on GaAs NWs was investigated. STEM measurements were performed to study the preferential accumulation of InAs on the NWs. Figure 3(a) shows the HAADF-STEM image of the upper region of the NW after InAs deposition. Due to the higher atomic number (Z) of In with respect to Ga, we attribute the regions with a brighter intensity to the presence of In(Ga)As clusters. These clusters are observed on the top facet (axial clusters) as well as along the NW side facets (radial clusters).

Figure 3(c) shows a magnified HAADF image of the GaAs NW tip after InAs deposition as indicated by a red rectangular region in figure 3(a). The corresponding In and Ga EDX maps are shown in figures 3(d) and (e). In(Ga)As clusters accumulate at the tip of the NW whereas, pure InAs accumulation is observed on both the inclined top facets. When the amount of InAs deposited is reduced, the InAs clusters become even smaller and are observed only on one of the inclined facets at the NW tip (supplementary information (https://stacks.iop.org/JOPT/22/084002/mmedia)). We

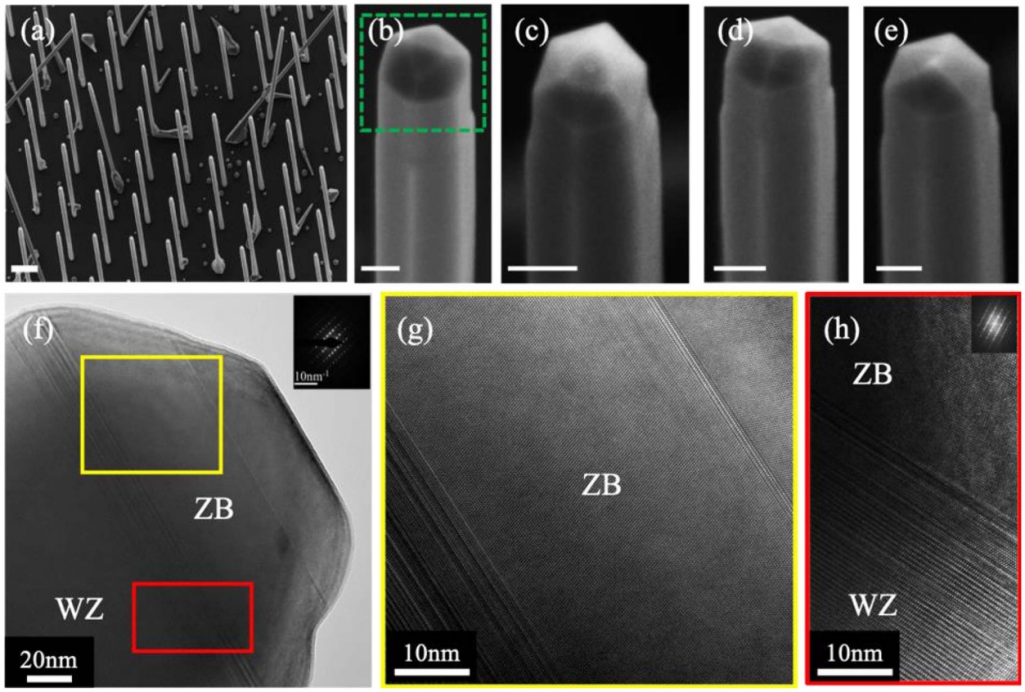

Figure 2. SEM and TEM image showing morphology of the nanowire sample with droplet consumption at 630 °C. (a) An overview of the NW array with 55 nm nanohole diameter and 2 μm pitch (inter-wire distance) (scale bar: 1 μm). (b)–(e) Magnified images of the resultant NW tip after the droplet consumption step (scale bars: 50 nm). (f)–(h) HR-TEM image of the NW tip taken along <1–10> zone axis. Insets in (f) and (h) show SAED patterns taken from the respective sections of the NW.

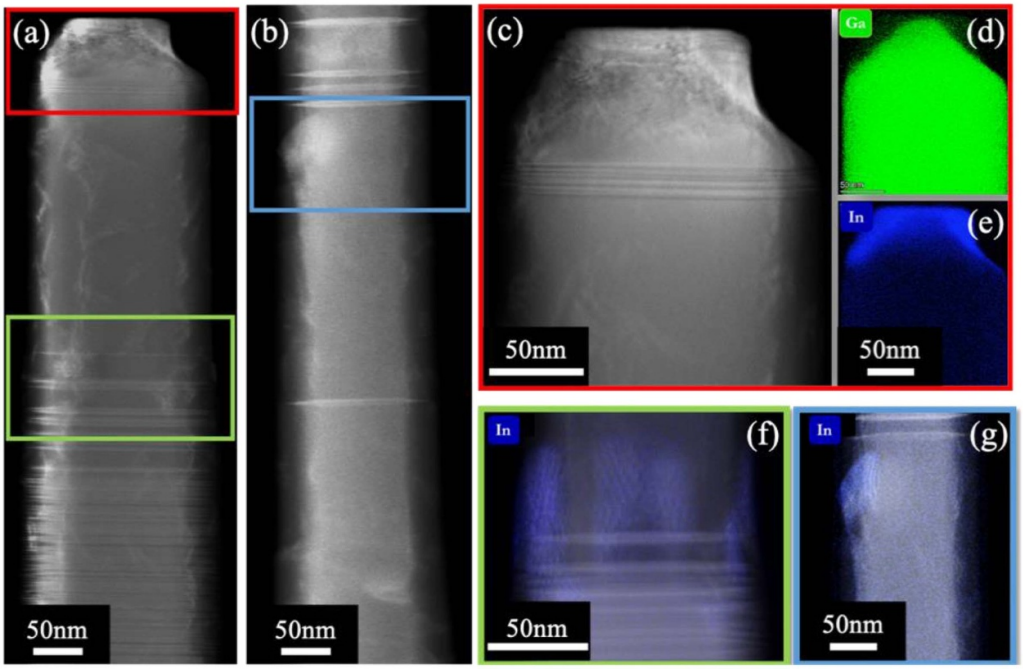

Figure 3. HAADF-STEM image of the GaAs NW tip after 5 s of InAs deposition under a V/III ratio of 45 at 630 °C. (a) HAADF image of the (a) upper (wurtzite) and (b) lower (zincblende) sections of the NW. (c) A magnified image of the NW tip and (d) and (e) simultaneous EDX elemental distributions of Ga and In, respectively. (f) and (g) HAADF-STEM images of two selected sections from the NW super imposed with the EDX map of In.

believe these smaller clusters on one of the inclined facets to be pure InAs based on the EDX maps of figures 3(d) and (e). However, we note that it is unclear at this point if the InAs clusters on the inclined top facets accumulate on one of the NW top facets or at the corner facet formed by the intersection of two crystal planes. This NW tip faceting is

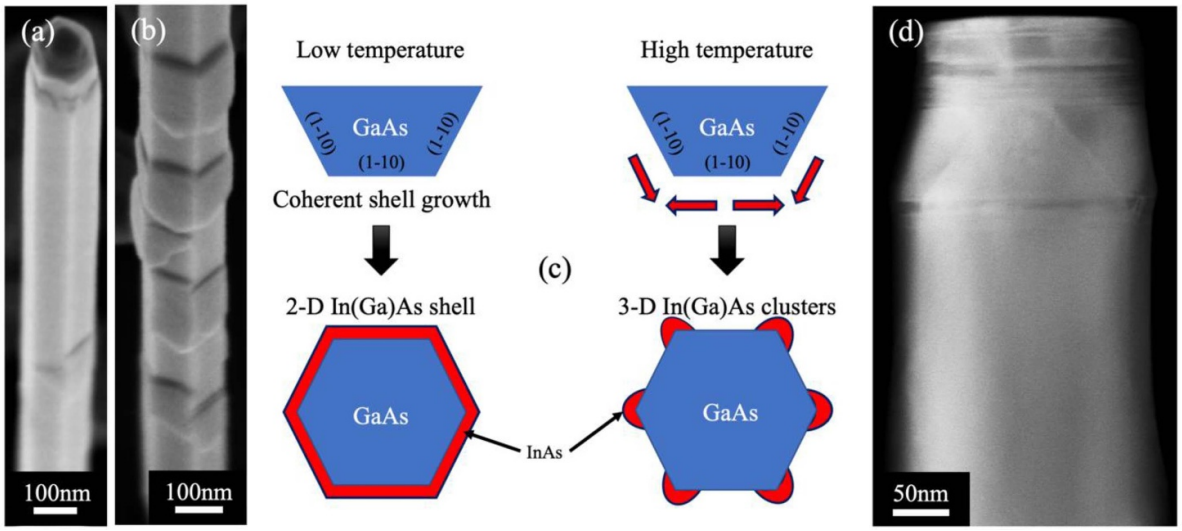

Figure 4. (a) and (b) SEM images of a NW sample after InAs deposition at low temperature (440 °C) for 5 mins. (c) Illustration of the proposed material transport mechanisms. The red arrow indicates the adatom diffusion driven by strain relaxation. (d) HAADF-STEM image of the tip of a NW taken from the sample with InAs deposition at high temperature after GaAs shell capping.

clearly evident from SEM images in figures 2(b)–(e). The InAs clusters accumulating on the corner facets at the tip are similar to the clusters nucleating at the corner facets on the NW sidewalls, as discussed in section 3.2. Further investigation is needed to determine the exact location of these clusters. This, however, shows that engineering of the NW top facet could help in obtaining axial InAs clusters.

3.2. Formation of radial In(Ga)As clusters:

Self-catalysed GaAs NWs commonly exhibit a hexagonal cross-section consisting of {1-10} type side facets connected by short {11-2} corner facets [26]. Three-dimensional growth of InAs nanostructures on GaAs (110) surfaces is found to be energetically unfavourable [27–30].

The Stranski-Krastonov growth of three-dimensional InAs islands on these surfaces has been realized only after covering the facets with a thin layer of surfactant material [28, 31]. In our case, we observe the formation of three-dimensional In-rich clusters on GaAs NW side facets by depositing InAs layer at a higher substrate temperature. In HAADF images of figures 3(a) and (b), which are taken along top and bottom parts of the NW, we observe regions with brighter contrast all along the NW sidewalls. This indicates the presence of radial In(Ga)As clusters along with axial clusters on GaAs NWs. This is also evident from the EDX elemental map of In overlapped with HAADF images of NW sidewalls in figures 3(f) and (g). The location of the observed In-rich radial clusters in figure 3(f) clearly suggests that they are nucleating on the edges separating the two {110} NW side facets.

In the following discussion, we propose a material transport model to explain the temperature-dependent formation of 3-D In(Ga)As clusters. We base our proposition on strain energy minimization. Strain energy minimization [32] and gradient in chemical potential [26] are the two known driving forces for adatom diffusion between different NW facets. The convex nature of the {11-2} corner facets makes them favourable sites for strain relaxation and the nucleation of 3-D structures [33]. At a higher substrate temperature, adatoms have enough kinetic energy to overcome the chemical potential barrier. Thus, material transport due to strain relaxation becomes dominant. This, in turn, promotes preferential accumulation of the impinging adatoms at the corner facets. This results in the formation of In-rich clusters along the {11-2} corner facets of the NW. A schematic of the proposed mechanism is shown in figure 4(c). At higher temperatures, In(Ga)As clusters preferentially accumulate at the corner facets indicated by red arrows, as observed in figure 3(f). In contrast, growth at a lower substrate temperature in the absence of a surfactant leads to the formation of a thin 2-D In(Ga)As shell [34]. Figures 4(a) and (b) show SEM images of upper and lower regions, respectively, of a NW sample grown at a lower substrate temperature (440 °C). The InAs deposition was carried out for 5 mins under an As_4 BEP of 5.6×10^{-6} Torr and a V/III ratio of 45. The formation of a thin discontinuous 2-D shell is observed. The lower diffusivity of In adatoms at this growth temperature leads to a high density of such clusters at the bottom of the NW (figure 4(b)) whereas a lower density is seen in the upper part of the NW (figure 4(a)).

3.3. Optical characterization of the In(Ga)As clusters:

To investigate the optical properties, CL and PL measurements were carried out on NW structures similar to the ones studied by STEM-EDX. However, to reduce the size of In(Ga)As clusters, InAs was deposited for 3 s under an In BEP of 2.2×10^{-8} Torr. The NWs were subsequently capped with a GaAs shell for confinement. The GaAs shell growth was carried out at a substrate temperature of 440 °C and under a high V/III ratio of 70 to ensure growth of a conformal 2-D GaAs shell. Ga and As_4 BEPs were maintained at 1.4×10^{-7} and 1.0×10^{-5} Torr, respectively. Figure 4(d) shows the HAADF

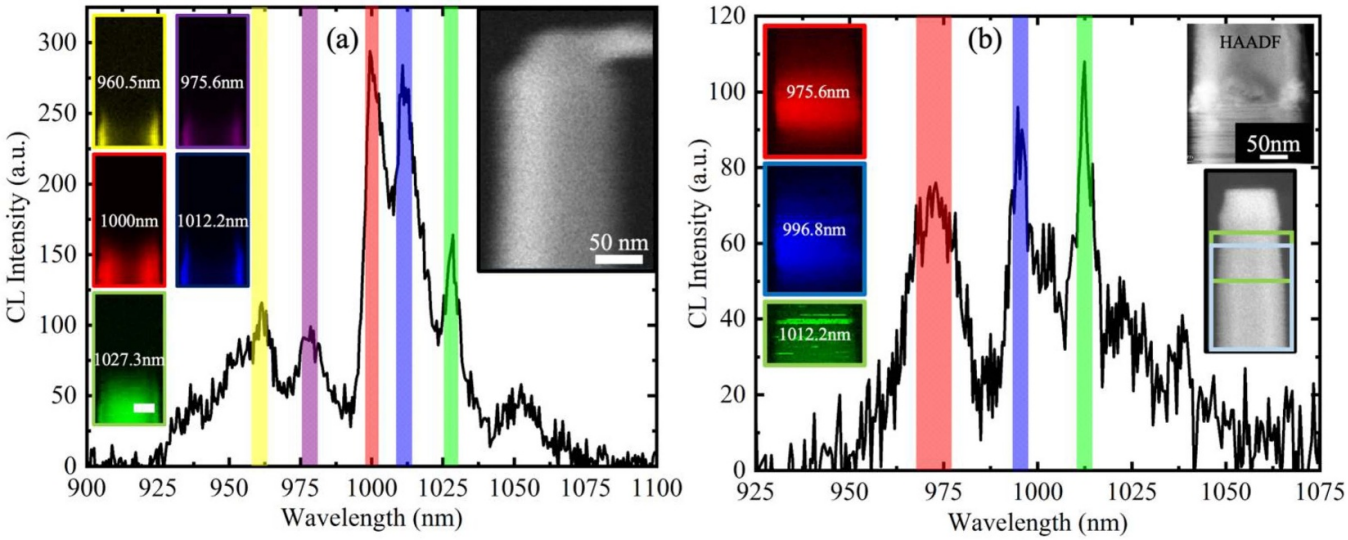

Figure 5. Spatially-averaged CL spectra of two representative NWs from the sample after shell capping. The spectra correspond to the emission averaged over the region close to the NW tips. The left and right insets indicate energy-filtered CL emission maps and CL-SEM images of the NWs respectively. The inset on the top right in (b) corresponds to a HAADF image of the region indicated by the green box.

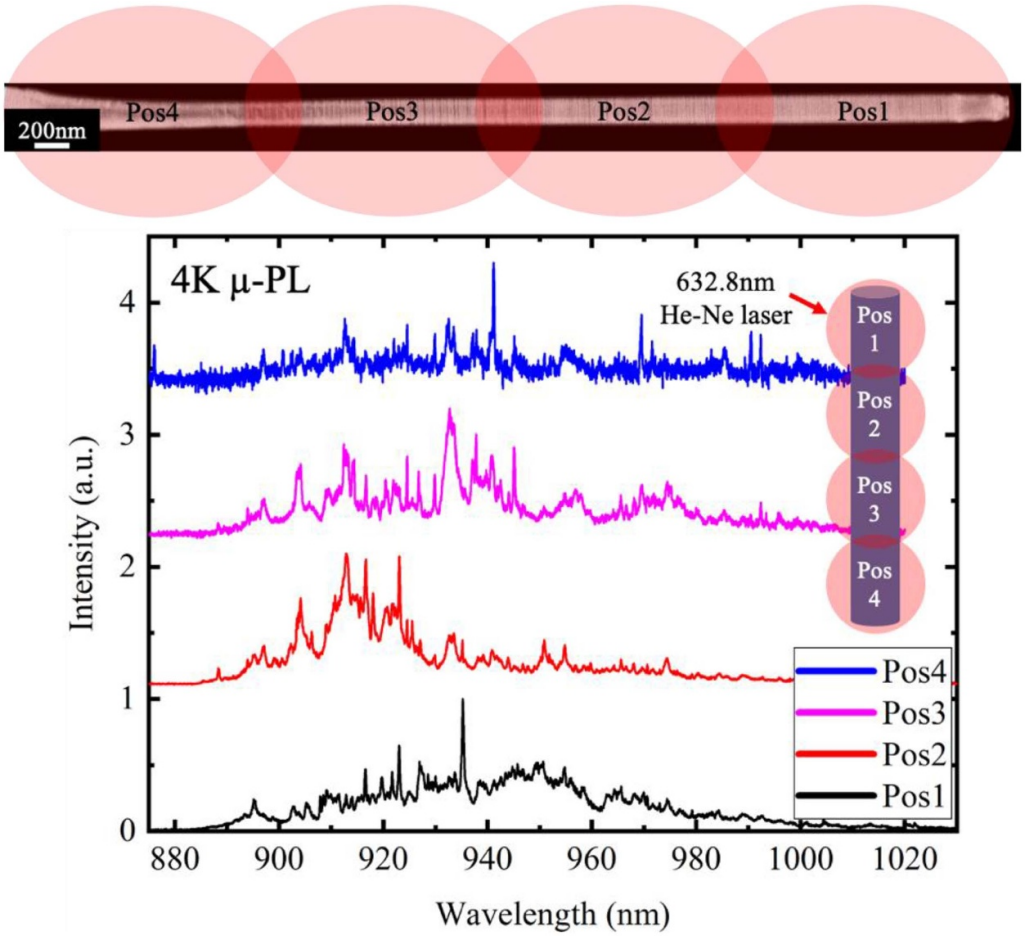

Figure 6. Micro-PL spectra acquired at 4 K from a NW lying horizontally on the as-grown substrate. The spectra are acquired at four different illumination positions on the NW as shown in the inset. The sharp peaks are a clear indication of quantized energy levels in the In(Ga)As clusters on the NW sidewalls.

image of a NW after shell capping. The tip of the NW showed a high density of defects upon capping with a GaAs shell. We also note that the HAADF contrast as seen in figure 3 from the In-rich clusters is not visible upon shell capping.

Figure 5 shows the CL spectra of two representative NWs from the sample after shell capping. The CL spectra correspond to the emission of a region close to the NW tip and are averaged through the region indicated in the SEM images in the insets. The insets on the left and the right show the energy-filtered CL maps and the SEM image of the NWs, respectively. The colour coding is mentioned on the respective energy-filtered CL maps in the insets. The spectra in figures 5(a) and (b) both show multiple peaks originating from different emission zones. Some emission zones appear as a strip across the whole NW diameter (1.207 eV) while others extend over very few pixels (1.225 eV, 1.24 eV, 1.271 eV, 1.291 eV). In agreement with the structural characterization results (figure 3), all the emission zones observed in the CL maps are in close proximity to each other. The emission zones in the CL maps of figure 5(a) are in agreement with the location of In(Ga)As clusters seen in figures 3(f) and (g). Due to the high density of defects at the tip, no emission is observed from this region of the NWs. In figure 5(b), the emission zones are near the stacking faults. This is evident from the emission map corresponding to 1.225 eV which indicates accumulation of In-rich clusters in the region with a high density of stacking faults. This is in agreement with the HAADF image in the inset of figure 5(b) where regions with brighter contrast are seen in the region full of stacking faults.

Due to the carrier diffusion length and excitation volume, the exact location of each localized clusters is challenging to resolve. However, the occurrence of multiple emission peaks suggests the presence of In-rich clusters all along the NW sidewalls. To confirm the presence of very thin In-rich clusters along the NW sidewalls, position-dependent PL measurements were carried out as shown in figure 6. The PL spectra were acquired from a single NW lying horizontally on the as-grown substrate. The background emission from the underlying substrate was absent and ensures that the spectra shown here indeed originate purely from the NW heterostructure. The spectra acquired at very low excitation powers reveal sharp QD-like emission lines. The narrow peaks with linewidths in the sub-meV range indicate that the emission originates from the In(Ga)As clusters confined on the NW sidewalls.

4. Conclusion

In summary, we have studied the effect of NW growth termination on the morphology of the GaAs NW tips obtained in ordered arrays. Depending on the NW morphology and growth temperature we have demonstrated the formation of axial and radial In(Ga)As clusters. GaAs NW tips showed a truncated pyramidal morphology with a flat triangular {111}B facet at the top. Moreover, the tips are found to be free of stacking faults and have a pure ZB crystal structure. In addition, In(Ga)As clusters were obtained all along the corner facets of the NW sidewalls. The occurrence of radial In(Ga)As clusters was confirmed by scanning TEM and low-temperature CL and PL measurements. We believe that the In(Ga)As cluster formation is driven by the convex nature of the {11-2} corner facets. This approach of facet-driven nanostructure self-assembly can be engineered to grow axial and radial QDs in lattice-mismatched NW heterostructures. In addition, they could also be exploited to make novel quantum structures ranging from 3-D islands to zig-zag shaped nano-rings on NWs [29]. The QD-in-nanowires could potentially contribute to single photon emitter devices with large repetition rates owing to small radiative decay lifetimes [35]. Considering the shortest excitonic lifetime measured in QD-in-nanowire systems (0.42 ns) [36], repetition rates could in principle be as high as 2 GHz. However, this high emission rate is only achievable by optical excitation. Challenges currently reside in the electrical excitation of QD-in-nanowires. Nonetheless, with the availability of sophisticated manipulation and processing techniques, the integration of nanowire QD emitters into silicon photonics operating at telecom wavelengths approaches the possible [37].

Acknowledgments

This work is part of a project that has received funding from the European Union's Horizon 2020 research and innovation programme under the Marie Skłodowska-Curie Grant Agreement No. 765075, LIMQUET project. Authors thank also INDEED project from the H2020 program. The authors also acknowledge funding received from SNF through Grant Nos. 40B2-0_176680, 200021_169908 as well as through the NCCR QSIT. A B and S P R thank Simon Escobar for help with electron microscopy. M N and C C would like to thank Robert Taylor and Régis Deturche for their help on the μ-PL setup.

ORCID iDs

A Balgarkashi https://orcid.org/0000-0003-0504-5542
A Fontcuberta i Morral https://orcid.org/0000-0002-5070-2196

References

[1] Mantynen H, Anttu N, Sun Z and Lipsanen H 2019 Single-photon sources with quantum dots in III-V nanowires *Nanophotonics* **8** 747–69
[2] Heiss M *et al* 2013 Self-assembled quantum dots in a nanowire system for quantum photonics *Nat. Mater.* **12** 439–44
[3] Panev N, Persson A I, Sköld N and Samuelson L 2003 Sharp exciton emission from single InAs quantum dots in GaAs nanowires *Appl. Phys. Lett.* **83** 2238–40
[4] Claudon J, Bleuse J, Malik N S, Bazin M, Jaffrennou P, Gregersen N, Sauvan C, Lalanne P and Gérard J M 2010 A highly efficient single-photon source based on a quantum dot in a photonic nanowire *Nat. Photonics* **4** 174–7
[5] Reimer M E, Bulgarini G, Akopian N, Hocevar M, Bavinck M B, Verheijen M A, Bakkers E P A M, Kouwenhoven L P and Zwiller V 2012 Bright single-photon sources in bottom-up tailored nanowires *Nat. Commun.* **3** 737

[6] Haffouz S *et al* 2018 Bright single InAsP quantum dots at telecom wavelengths in position-controlled InP nanowires: the role of the photonic waveguide *Nano Lett.* **18** 3047–52

[7] Dalacu D, Mnaymneh K, Wu X, Lapointe J, Aers G C, Poole P J and Williams R L 2011 Selective-area vapor-liquid-solid growth of tunable InAsP quantum dots in nanowires *Appl. Phys. Lett.* **98** 251101

[8] Nötzel R, Temmyo J, Kozen A, Tamamura T, Fukui T and Hasegawa H 1996 Self-organized growth of quantum-dot structures *Solid State Electron.* **40** 777–83

[9] Francaviglia L, Fontana Y and Fontcuberta I Morral A 2016 Quantum dots in nanowires *Semiconductor Nanowires II: Properties and Applications* vol 94 (Amsterdam: Elsevier) pp 159–84

[10] Friedler I, Sauvan C, Hugonin J P, Lalanne P, Claudon J and Gérard J M 2009 Solid-state single photon sources: the nanowire antenna *Opt. Express* **17** 2095

[11] Fontcuberta I Morral A 2011 Gold-free GaAs nanowire synthesis and optical properties *IEEE J. Sel. Top. Quantum Electron.* **17** 819–28

[12] McIntyre P C and Fontcuberta I Morral A 2020 Semiconductor nanowires: to grow or not to grow? *Mater. Today Nano* **9** 100058

[13] De La Mata M, Magén C, Caroff P and Arbiol J 2014 Atomic scale strain relaxation in axial semiconductor III-V nanowire heterostructures *Nano Lett.* **14** 6614–20

[14] Aharonovich I, Englund D and Toth M 2016 Solid-state single-photon emitters *Nat. Photonics* **10** 631–41

[15] Yan Z X and Milnes A G 1982 Deep level transient spectroscopy of silver and gold levels in LEC grown gallium arsenide *J. Electrochem. Soc.* **129** 1353

[16] Li N, Tan T Y and Gösele U 2008 Transition region width of nanowire hetero- and pn-junctions grown using vapor-liquid-solid processes *Appl. Phys.* A **90** 591–6

[17] Dick K A, Kodambaka S, Reuter M C, Deppert K, Samuelson L, Seifert W, Wallenberg L R and Ross F M 2007 The morphology of axial and branched nanowire heterostructures *Nano Lett.* **7** 1817–22

[18] McIntyre P C and Fontcuberta I Morral A 2019 Semiconductor nanowires: to grow or not to grow? *Mater. Today Nano* **9** 100058

[19] Glas F, Harmand J-C and Patriarche G 2007 Why does wurtzite form in nanowires of III-V zinc blende semiconductors? *Phys. Rev. Lett.* **99** 146101

[20] Yu X, Wang H, Lu J, Zhao J, Misuraca J, Xiong P and Von Molnár S 2012 Evidence for structural phase transitions induced by the triple phase line shift in self-catalyzed GaAs nanowires *Nano Lett.* **12** 5436–42

[21] Tersoff J 2015 Stable self-catalyzed growth of III-V nanowires *Nano Lett.* **15** 6609–13

[22] Panciera F, Baraissov Z, Patriarche G, Dubrovskii V G, Glas F, Travers L, Mirsaidov U and Harmand J 2020 Phase selection in self-catalyzed GaAs nanowires *Nano Lett.* **3** 1669

[23] Priante G, Ambrosini S, Dubrovskii V G, Franciosi A and Rubini S 2013 Stopping and resuming at will the growth of GaAs nanowires *Cryst. Growth Des.* **13** 3976–84

[24] Dubrovskii V G, Xu T, Álvarez A D, Plissard S R, Caroff P, Glas F and Grandidier B 2015 Self-equilibration of the diameter of Ga-catalyzed GaAs nanowires *Nano Lett.* **15** 5580–4

[25] Rudolph D, Schweickert L, Morkötter S, Hanschke L, Hertenberger S, Bichler M, Koblmüller G, Abstreiter G and Finley J J 2013 Probing the trapping and thermal activation dynamics of excitons at single twin defects in GaAs-AlGaAs core-shell nanowires *New J. Phys.* **15** 113032

[26] Jeon N, Ruhstorfer D, Döblinger M, Matich S, Loitsch B, Koblmueller G and Lauhon L J 2018 Connecting composition-driven faceting with facet-driven composition modulation in GaAs-AlGaAs core-shell nanowires *Nano Lett.* **18** 5179

[27] Lewis R B, Corfdir P, Herranz J, Küpers H, Jahn U, Brandt O and Geelhaar L 2017 Self-assembly of InAs nanostructures on the sidewalls of GaAs nanowires directed by a Bi surfactant *Nano Lett.* **17** 4255–60

[28] Dimakis E, Jahn U, Ramsteiner M, Tahraoui A, Grandal J, Kong X, Marquardt O, Trampert A, Riechert H and Geelhaar L 2014 Coaxial multishell (In,Ga)As/GaAs nanowires for near-infrared emission on Si substrates *Nano Lett.* **14** 2604–9

[29] Lähnemann J *et al* 2019 Correlated nanoscale analysis of the emission from wurtzite versus zincblende (In,Ga)As/GaAs nanowire core-shell quantum wells *Nano Lett.* **19** 4448–57

[30] Belk J G, Pashley D W, McConville C F, Sudijono J L, Joyce B A and Jones T S 1997 Surface atomic configurations due to dislocation activity in InAs/GaAs(110) heteroepitaxy *Phys. Rev.* B **56** 10289–96

[31] Uccelli E, Arbiol J, Morante J R and Fontcuberta I Morral A 2010 InAs quantum dot arrays decorating the facets of GaAs nanowires *ACS Nano* **4** 5985–93

[32] Lewis R B, Nicolai L, Küpers H, Ramsteiner M, Trampert A and Geelhaar L 2017 Anomalous strain relaxation in core-shell nanowire heterostructures via simultaneous coherent and incoherent growth *Nano Lett.* **17** 136–42

[33] Yang B, Liu F and Lagally M G 2004 Local strain-mediated chemical potential control of quantum dot self-organization in heteroepitaxy *Phys. Rev. Lett.* **92** 025502

[34] Herranz J *et al* 2020 Coaxial GaAs/(In,Ga)As dot-in-a-well nanowire heterostructures for electrically driven infrared light generation on Si in the telecommunication O band *ACS Appl. Nano Mater.* **3** 165–74

[35] Deshpande S, Heo J, Das A and Bhattacharya P 2013 Electrically driven polarized single-photon emission from an InGaN quantum dot in a GaN nanowire *Nat. Commun.* **4** 1675

[36] Borgström M T, Zwiller V, Müller E and Imamoglu A 2005 Optically bright quantum dots in single nanowires *Nano Lett.* **5** 1439–43

[37] Zadeh I E, Elshaari A W, Jöns K D, Fognini A, Dalacu D, Poole P J, Reimer M E and Zwiller V 2016 Deterministic integration of single photon sources in silicon based photonic circuits *Nano Lett.* **16** 2289–94